Mechatronics 106 (2025) 103287

Contents lists available at ScienceDirect

Mechatronics

journal homepage: www.elsevier.com/locate/mechatronics

Using Franka Emika collaborative robot as a haptic device ☆

Wilson Brian, Sebastián Gutiérrez, Jorge Juan Gil *

Department of Mechanical Engineering, Tecnun, University of Navarra, San Sebastián, E-20018, Guipúzcoa, Spain

ARTICLE INFO

Keywords:
Collaborative robot
Haptic device
Impedance analysis

ABSTRACT

This study investigates the feasibility of using a collaborative robot as a haptic device. The research analyzes the robot's behavior across a range of frequencies relevant to human interaction under two opposite operating conditions: free movement and highly constrained movement. To characterize the robot's performance, simplified models are estimated. The resulting dynamics is compared with those of other mechanisms specifically designed for haptic rendering. The study identifies two key challenges: the anisotropy of the apparent inertia and the presence of resonance. In particular, resonance in constrained motion results in a reduced perceived impedance, deviating from the sensation of rigid contact. In order to address this issue, the study examines the application of viscosity to dampen resonance and improve user experience. The findings indicate that with appropriate adjustments and control techniques, a collaborative robot can indeed serve as a haptic device, offering comparable performance to that of specialized haptic mechanisms.

1. Introduction

In recent years, collaborative robots have emerged as versatile tools that can be operated by human users with minimal effort, as if they were backdrivable mechanisms. This feature makes them suitable for use as haptic devices that provide force feedback to the user by replicating the forces and torques of a given application. Haptic interfaces are widely used in two primary domains: virtual environments and teleoperation.

In virtual environments, haptic feedback offers a level of realism that surpasses what visual stimuli alone can achieve. This increases the user's immersion in the task being performed, which improves the effectiveness of its use for training motor tasks [1], which, in addition to representing virtual objects, can exert forces to guide and constrain the user's movement [2] in optimal trajectories. In addition, haptic feedback finds applications in collaborative tasks and medical rehabilitation [3], where the device not only directs, but also amplifies the user's effort or accuracy.

In teleoperation, haptic interfaces enable users to perform tasks remotely, allowing interventions in inaccessible or hazardous environments while minimizing operator risk [4]. This capability is especially valuable in scenarios such as robotic surgery, where precision and reduced invasiveness yield significant benefits for patients [5].

The operation of haptic devices relies on two principal control methodologies: impedance control and admittance control. Impedance control generates forces dependent to the user-induced motion, allowing the user to perceive the dynamic characteristics of the device. In contrast, admittance control adjusts the device's position in response to the force exerted by the operator. Both methods have their respective strengths and trade-offs in terms of accuracy, responsiveness, and realism in haptic interactions [6].

A critical factor in the design of haptic devices is transparency–the extent to which the user perceives the simulated interaction properties accurately and without interference from the device's own dynamics [7]. In free motion, this means that the dynamics of the device should "disappear", exhibiting minimal friction, inertia, or other dynamic effects. Conversely, when interacting with rigid virtual or remote objects, the device must provide high impedance to replicate physical constraints. The range of impedances that a device can render is known as its Z-width [8], a parameter often evaluated using Bode diagrams.

Despite the promising potential of haptic devices, many commercially available systems, designed primarily for desktop use, face limitations in size, force capacity, and workspace. These constraints hinder their suitability for some industrial applications. Collaborative robots, with their superior load capacity, large workspaces, and integrated force/torque sensors, offer a compelling alternative [6]. However, their mechanical transparency remains an area requiring further investigation. For instance, [9] demonstrated the application of a Kuka collaborative robot in high-force scenarios but did not analyze its transparency performance.

☆ This paper was recommended for publication by Associate Editor Maurizio Porfiri.

* Corresponding author.
E-mail addresses: wbrianmesa@unav.es (W. Brian), jsgutierrez@unav.es (S. Gutiérrez), jjgil@unav.es (J.J. Gil).

https://doi.org/10.1016/j.mechatronics.2024.103287
Received 8 August 2024; Received in revised form 12 November 2024; Accepted 4 December 2024
Available online 13 December 2024

Table 1
Specifications of the Franka Emika robot arm.

Feature	Value		
Degrees of freedom	7		
Payload	3 kg		
Reach	850 mm		
Repeatability	+/- 0.1 mm (ISO 9283)		
Weight	~18 kg		
Joint limits	J1	−166°/166°	150 °/s
	J2	−101°/101°	150 °/s
	J3	−166°/166°	150 °/s
	J4	−176°/-4°	150 °/s
	J5	−166°/166°	180 °/s
	J6	−1°/215°	180 °/s
	J7	−166°/166°	180 °/s

Table 2
Denavit–Hartenberg parameters of the robot arm.

Joint	θ_i (rad)	d_i (m)	a_i (m)	α_i (rad)
1	q_1	0.333	0	$-\pi/2$
2	q_2	0	0	$\pi/2$
3	q_3	0.316	0.0825	$\pi/2$
4	q_4	0	−0.0825	$-\pi/2$
5	q_5	0.384	0	$\pi/2$
6	q_6	0	0.088	$\pi/2$
7	q_7	0.107	0	0

This work explores the possibility of using the Franka Emika robot as a haptic device, assessing its performance based on user perception. In particular, its characteristics are analyzed in two extreme situations: free motion and constrained motion. The paper is organized as follows: Section 2 provides an overview of the Franka Emika robot's features. Section 3 and IV examine its performance in free and constrained motion, respectively. Section 5 discusses the results and compares them with other haptic devices. Finally, Section 6 presents conclusions and future research directions.

2. Franka Emika robot

The Franka Emika is a 7-axis robot arm with a payload capacity of 3 kg and a reach of 850 mm. Its repeatability is ±0.1 mm, and the robot weights approximately 18 kg. Table 1 provides the specifications of the robot arm [10]. Fig. 1 shows the kinematic model of the robot with the Denavit–Hartenberg parameters detailed in Table 2 [11].

To enhance the usability and functionality of the Franka Emika robot as a haptic device, an ergonomic handle was designed. This handle prioritizes energy efficiency by carefully balancing key measurements, including the handle's diameter, length, and side button dimensions. Drawing insights from a study on hand tool design by the Canadian Centre of Health and Safety [12], which recommends a handle diameter of 30–50 mm for force and stability and 8–16 mm for precise control, a balance was sought between precision and force efficiency. This balance led to a handle diameter of approximately 28 mm, ensuring optimal performance across various tasks. Additionally, the recommended handle length should exceed 100 mm for ease of use [12]. The final handle length was determined to be 120 mm, which facilitates ease of grip-switching, accommodating diverse user preferences.

The design was subsequently produced through 3D printing, integrating it with the Franka Emika robot. The final product is shown in Fig. 2, and the detailed blueprint for the handle dimensions is available in the provided file set [13]. Fig. 3 shows a user interacting with the device in a standard operational position, used consistently across the experiments discussed in the following sections.

A possible application for this system is enabling haptic interaction with virtual or remote environments that require the restitution of forces and torques within a wide workspace. The handle is designed

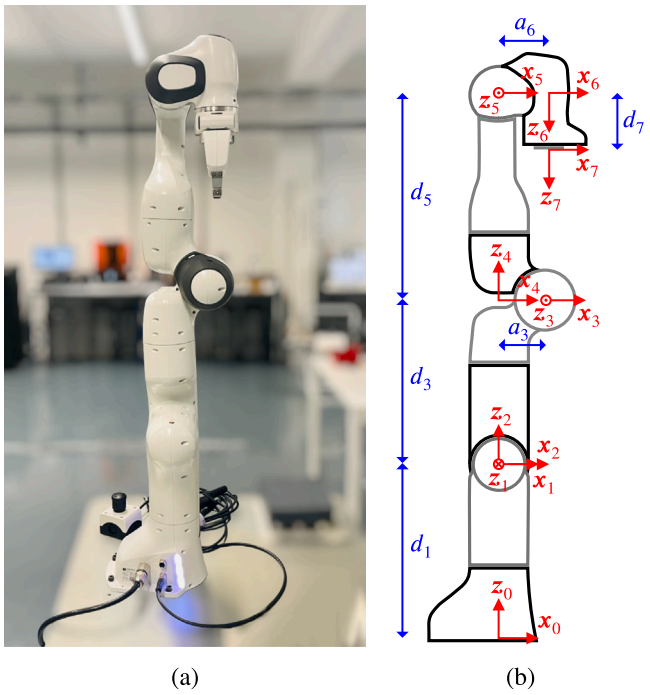

Fig. 1. (a) Franka Emika robot in zero position, (b) kinematic model of the robot arm.

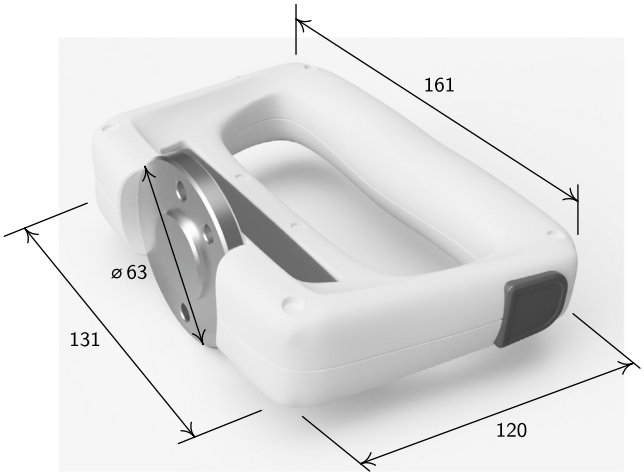

Fig. 2. 3D handle designed for the Franka Emika robot, dimensions in millimeters.

for ambidextrous use, making it suitable for both right- and left-handed users. Depending on the way the handle is grasped, it can function as a joystick. When held as shown in Fig. 3, the handle is well-suited for tasks such as cleaning, polishing, and grinding, making it applicable in various manual and precision tasks in industry.

3. Apparent dynamics in free motion

To operate the robot in free motion, the manufacturer's internal control models compensate for gravity, Coriolis and friction forces. In this operating mode, in which the system does not compensate for its own inertia or viscosity, the user tests the performance of the robot.

Due to the size of the robot, high apparent inertia could be expected. In addition, as a serial mechanism, there should be anisotropy when moving the device in different directions starting from the same position, as shown in Fig. 3. To verify these observations, it is necessary to

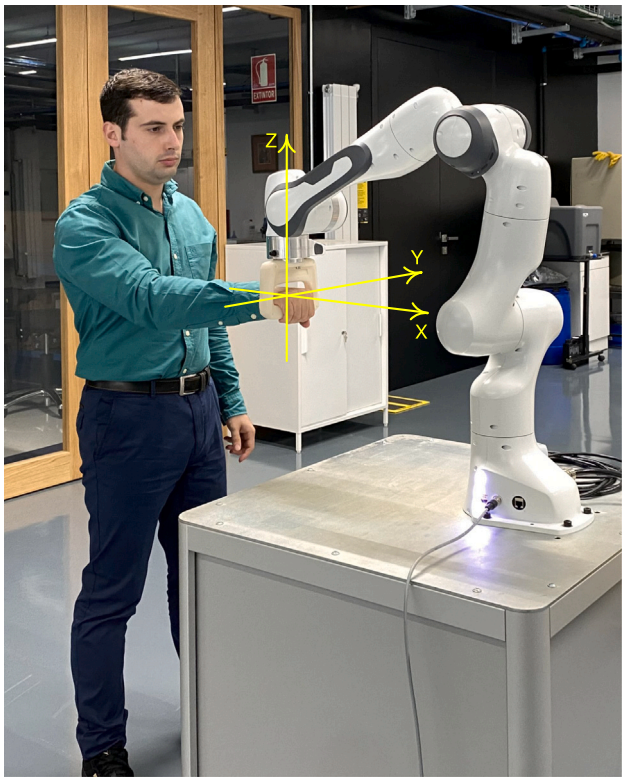

Fig. 3. User manipulating the robot.

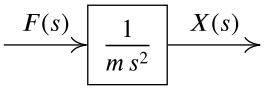

Fig. 4. Apparent inertia in free motion.

study the mechanical behavior and estimate the apparent dynamics of the device.

Like other collaborative robots, the Franka Emika robot is equipped with joint torque sensors to estimate the force exerted by the user. This measure and the displacement are used in this work to estimate the dynamics of the system. Consequently, no additional equipment or sensors are required, as they could alter the system's natural behavior. This experimental setup, in which the human operator directly manipulates the robot, closely resembles the intended use of the robot as a haptic interface.

The user's force is desired to be projected in the Cartesian directions shown in Fig. 3, which define a global, fixed eternal frame where the Z-axis points vertically upward and the X-axis vector points to the front of the user. The robot can provide the user's forces in the base frame $\{\mathbf{x}_0, \mathbf{y}_0, \mathbf{z}_0\}$ (Fig. 1). The Z-axis coincides with the direction of $\mathbf{z}_0$ and the X- and Y-axes point in the opposite directions to $\mathbf{x}_0$ and $\mathbf{y}_0$, respectively. The force measurements provided by the Franka Emika robot are well-conditioned and have low noise levels, thanks to internal filters that introduce a brief delay in the force signal. This delay can be canceled offline as suggested in [14].

3.1. Experimental analysis

To describe the experimental methods, we assume that the apparent dynamics in free motion consists solely of inertia (Fig. 4). If this assumption hold true, the relationship between the force applied by the user and the resulting displacement is predictable.

According to Newton's second law, force is the second derivative of displacement. Thus, applying a constant force (a step input) should produce a parabolic response:

$$f(t) = f_0 \quad \Rightarrow \quad x(t) = \frac{f_0}{2m} t^2 \tag{1}$$

The inertia can be estimated with a single experiment by knowing the input force and the curvature of the response. Other input profiles may also be considered. For instance, if the user applies a sinusoidal force:

$$f(t) = f_0 \sin(\omega t) \tag{2}$$

The resulting acceleration will be proportional to the force:

$$a(t) = \frac{1}{m} f(t) = \frac{f_0}{m} \sin(\omega t) \tag{3}$$

When integrated, the velocity and displacement become sinusoidal as well:

$$v(t) = -\frac{f_0}{m\omega} \cos(\omega t) \tag{4}$$

$$x(t) = -\frac{f_0}{m\omega^2} \sin(\omega t) \tag{5}$$

Force and displacement are in counterphase (one signal is delayed π radians with respect to the other):

$$x(t) = \frac{f_0}{m\omega^2} \sin(\omega t + \pi) = -\frac{1}{m\omega^2} f(t) \tag{6}$$

Again, the apparent inertia can be estimated with a single experiment by knowing the amplitude of both sinusoidal signals and the oscillation frequency.

Although either experiment described could be used to estimate inertia, the sinusoidal profile is preferable, as inertia can vary significantly throughout the robot's workspace. The sinusoidal profile is confined in a limited spatial area, while the parabolic profile is not.

Human operators cannot easily exert forces with precise shapes. For this reason, the input and output signals are analyzed in the frequency domain. If the force amplitude f_0 remains constant and the user increases the oscillation frequency ω, the displacement amplitude decreases with the square of the frequency. This relationship appears as a slope of −40 dB/decade in the gain Bode plot. Conversely, if the displacement amplitude is held constant, force amplitude must increase with the square of ω.

In this paper, to estimate the system dynamics, the user applies an oscillatory motion with increasing frequency, similar to a chirp function. Since the input and output signals are analyzed in the frequency domain, the user's input signal could follow any profile, as long as it contains information within a known bandwidth. However, the human-generated chirp signal clearly shows the frequency range in which the user can apply voluntary movements.

Fig. 5 presents the vertical component of force exerted by the user and the displacement in that direction. The observed behavior is consistent with an inertial dynamics because (i) the force and displacement are nearly in counterphase, and (ii) the amplitude of the force increases with the oscillation frequency while the amplitude of the displacement remains almost constant. Using `tfestimate` Matlab command, it is possible to obtain the experimental frequency response of the system (the Bode diagram) in the range of frequencies that are covered by the user.

Fig. 6 shows the frequency response of the robot in free motion along the vertical direction. As expected, the relationship between force and displacement is mainly characterized by an inertial effect (a slope of −40 dB/decade around 1 Hz). However, a viscous damping effect is necessary to explain the change in slope at low frequencies, and phase increase. Thus, the proposed apparent dynamics of the system for the frequency range in which the user can perform voluntary movements

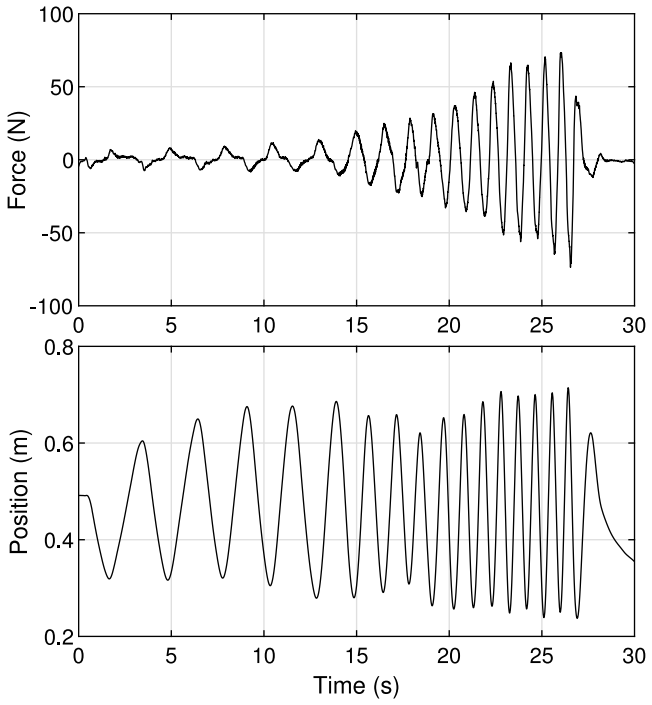

Fig. 5. Measured force and displacement along Z-axis.

is

$$G(s) = \frac{1}{m\,s^2 + b\,s}, \tag{7}$$

where m and b are the inertia and the viscous damping coefficient, respectively. Through the least squares method, in the range between 0.5 and 3 Hz, the resulting estimated parameters are $m = 4.21$ kg and $b = 10.73$ Ns/m. The proposed dynamics for the system (7) using the fitted parameters is also shown in Fig. 6.

3.2. Isotropy analysis

Although the fit presented in Fig. 6 is accurate, it cannot be stated that the apparent dynamics of the robot is the same at all points of its workspace. Moreover, even if the user mainly handled the robot close to the position shown in Fig. 3 (centered in the workspace) the apparent inertia in free motion may vary depending on the direction of movement. For this reason, we have carried out some experiments to analyze whether the robot's behavior is isotropic depending on the direction of movement or not.

The frequency responses along the three Cartesian directions are presented in Fig. 7. The apparent inertia along the Y-axis is similar to that of the Z-axis, while that along the X-axis is considerably greater, with an estimated value of 12.85 kg. In general, when the user operates the robot in the center of the workspace, similar results have been obtained: an apparent inertia between 4 and 5 kg in the Z-Y plane and a little more than 10 kg in the X axis. The anisotropy detected in the apparent inertia is likely due to how the robot links actually reconfigure and move.

Anyone who has manipulated a collaborative robot understands that the effort required to move the mechanism varies on the direction, even starting from the same pose. In this section we have shown a simple way to determine the apparent inertia of the robot in free movement: translate the force and position signals into frequency response, and observe the altitude at which −40 dB/decade line appears.

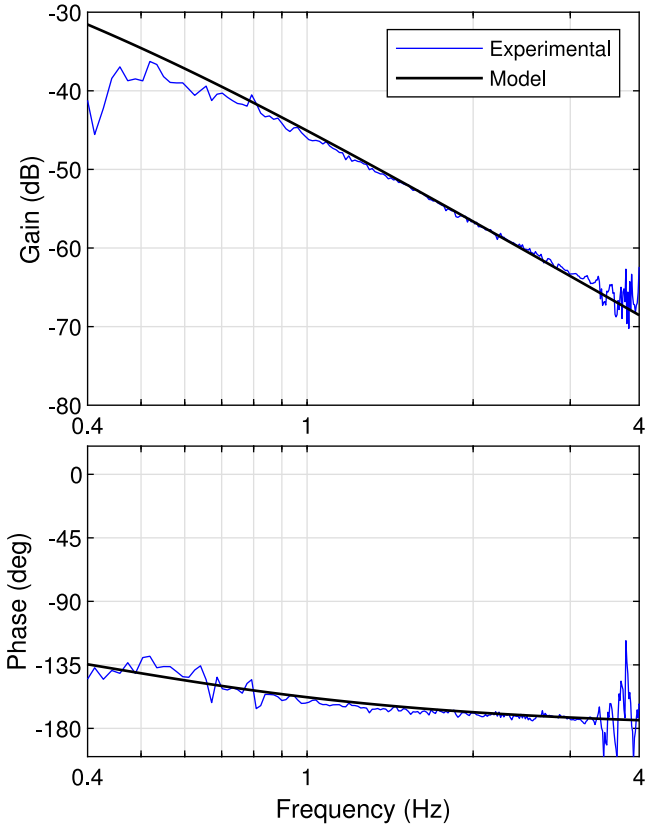

Fig. 6. Experimental frequency response along Z-axis and fitted model.

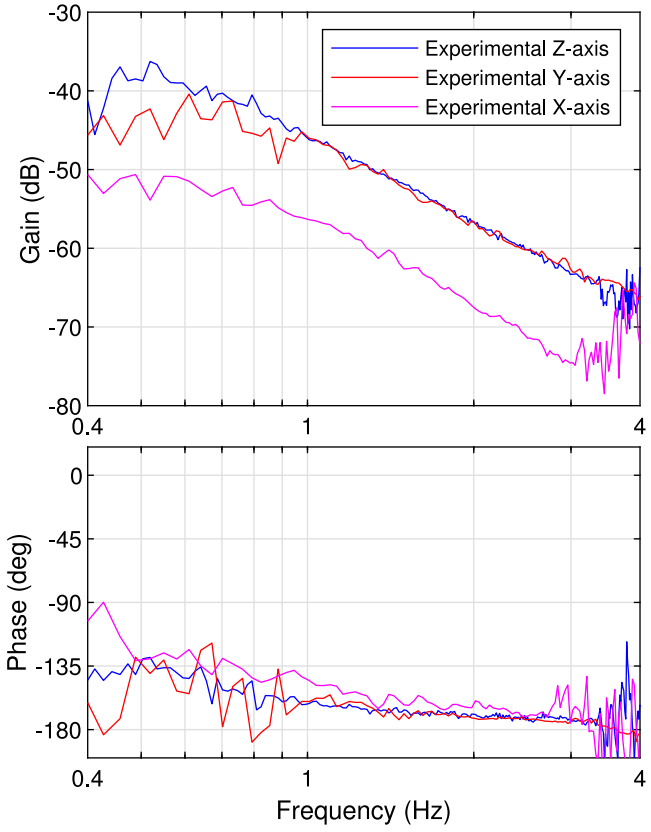

Fig. 7. Experimental frequency responses along the three Cartesian axis.

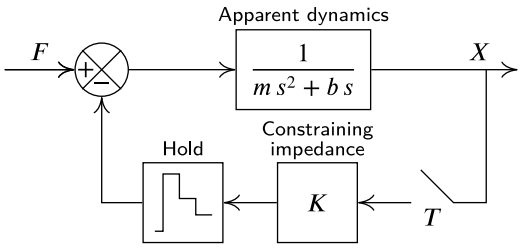

Fig. 8. Impedance loop to constrain the motion.

4. High impedance constrained motion

This section faces the opposite situation to free motion, that is, the movement is constrained by a virtual impedance. These impedances are position-depend and, among them, the simplest is the elastic effect with high stiffness coefficient, that is, a force proportional to the displacement (Fig. 8).

Although the impedance is implemented in discrete time, below the Nyquist frequency the user feels a simple mass–spring–damper dynamics:

$$G(s) \approx \frac{1}{m\,s^2 + b\,s + K} \tag{8}$$

Stiffness values K that are common in haptic applications simulating contact with rigid virtual walls will be analyzed. The stability of the human–machine interaction imposes a limit–a critical stiffness–, which is usually much lower than the stiffness of real metallic objects. According to [15], the critical stiffness values of the Impulse Engine, the Phantom, the Freedom 6 and the MIT Toolhandle are 800, 1015, 2400 and 3125 N/m respectively. For safety reasons, the values implemented in haptic simulations are lower than the critical ones. Considering this, five indicative stiffness values will be analyzed: 600, 800, 1000, 1200 and 1400 N/m.

If apparent inertia m and damping b were correctly estimated in Section 3, the system should exhibit a predictable behavior when implementing a specific stiffness K. Fig. 9 shows the theoretical frequency responses of constrained dynamics (8) using $m = 5$ kg and $b = 10$ Ns/m for the robot and the five indicative stiffness coefficients.

This behavior is corroborated experimentally. Similar to the procedure performed in Section 3, the system is manually excited in the Z-axis by incorporating five stiffness coefficients: 600, 800, 1000, 1200 and 1400 N/m. Fig. 10 shows the force that the user exerts and the displacement in that vertical direction using $K = 1000$ N/m. The measured signals are compatible with the proposed dynamics (8) because (i) the force and the displacement are nearly in phase at low frequencies, meaning that the force is proportional to the position, and (ii) a resonance peak appears near 2 Hz.

The behavior becomes evident when the signals are combined to plot the frequency response of the system (Fig. 11). The experimental results fit very well with the theoretical model (Fig. 9). Therefore, we can consider the estimated values for m and b and the dynamics (8) as valid.

Three areas have been highlighted in Figs. 10 and 11. At very low frequencies (zone I) the proportional relationship between force and displacement is directly the constant K of the stiffness. Around the resonance peak (zone II), with very little effort a relatively large displacement can be maintained. Above the resonance frequency (zone III), more and more force is needed. In our opinion, the existence of such a pronounced resonance peak is detrimental to haptic interaction. The goal of adding the impedance is to prevent the user from moving, as in contact with a rigid object. No one expects to feel a significant bouncing effect pushing a wall. In fact, in resonance zone II, the user feels that he/she is interacting with the relatively small mass of the second-order system (8).

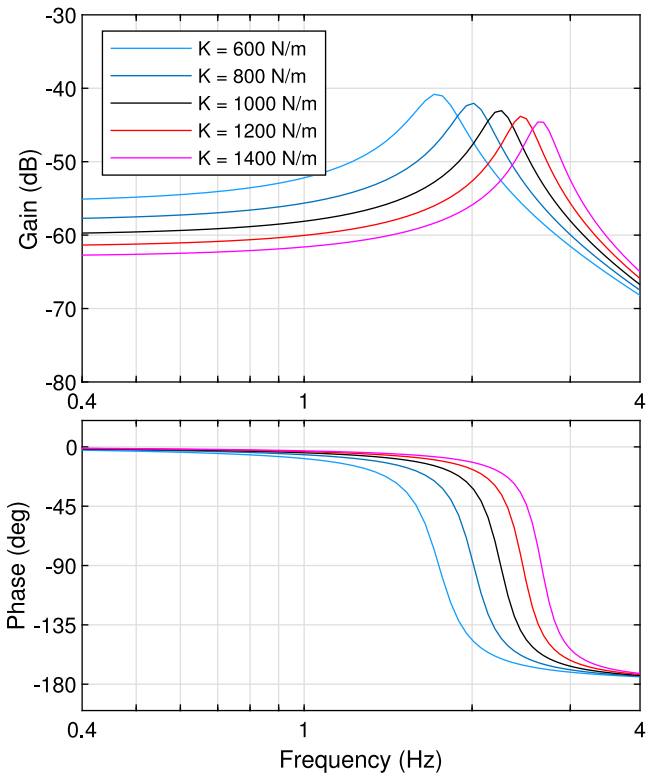

Fig. 9. Theoretical frequency responses with elastic effect.

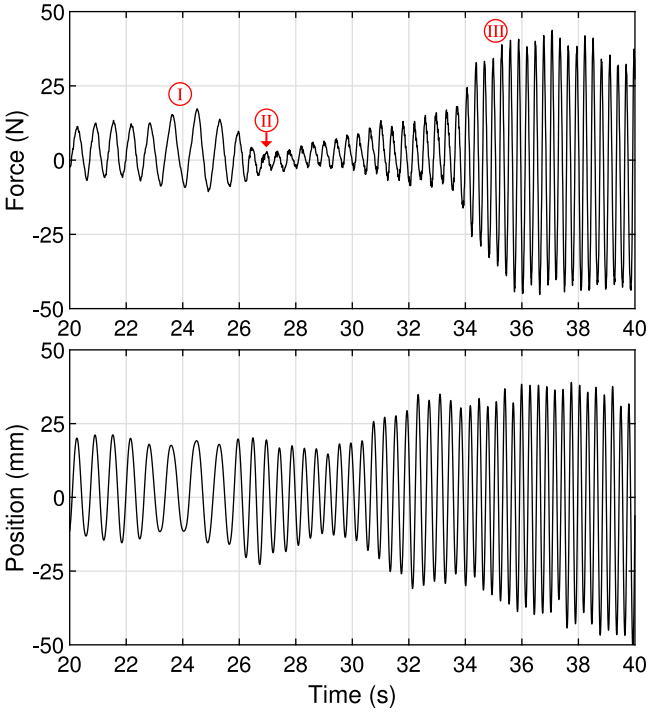

Fig. 10. Measured force and displacement along Z-axis in case of constrained motion with elastic impedance.

To compensate for this undesired effect, and to improve motion restriction, a virtual damping B is added to the impedance (Fig. 12).

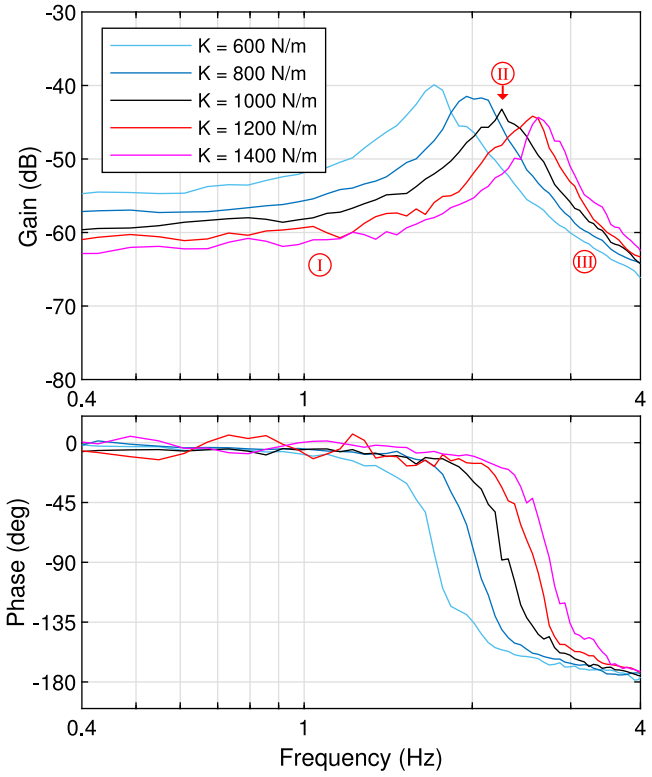

Fig. 11. Experimental frequency responses with elastic effect.

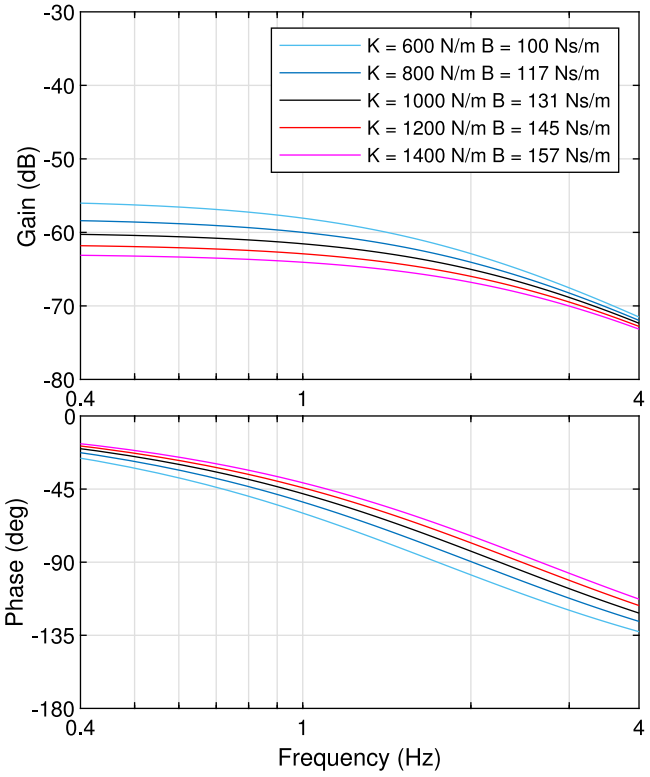

Fig. 13. Theoretical frequency response of the system with viscoelastic impedances.

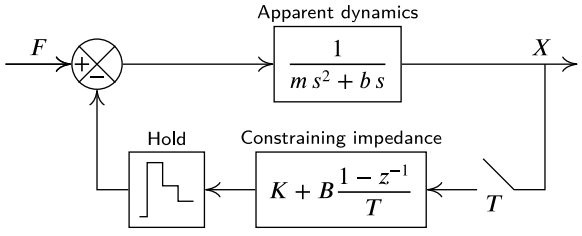

Fig. 12. Impedance loop to constrain the motion.

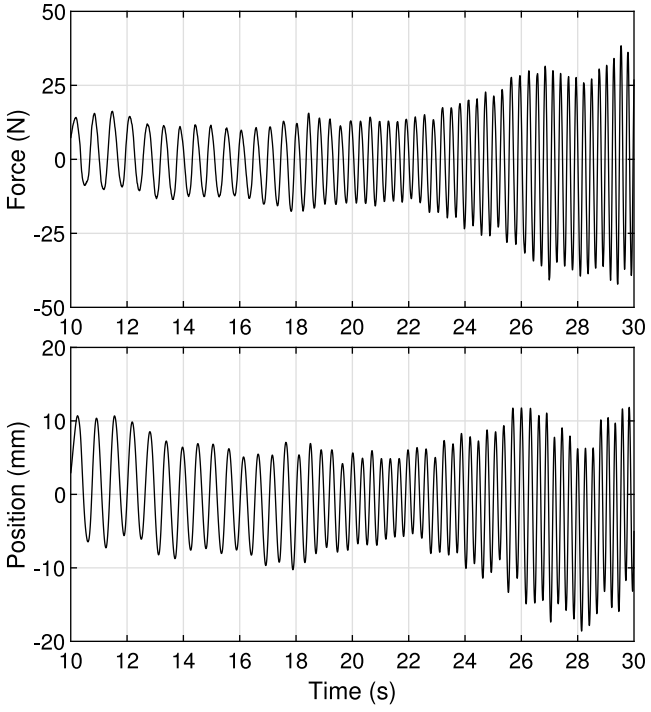

Fig. 14. Measured force and displacement along Z-axis in case of constrained motion with viscoelastic impedance.

Again, below the Nyquist frequency, system dynamics can be approximated as a second-order transfer function,

$$G(s) \approx \frac{1}{m\,s^2 + (b + B)\,s + K}. \tag{9}$$

For each stiffness coefficient K, virtual damping B can be selected to remove the resonance peak, that is, to achieve a second-order system with critical damping ($\zeta = 1$). This approach requires the values of apparent inertia and damping that have been previously estimated:

$$B = \sqrt{4\,m\,K} - b \tag{10}$$

To check experimentally if the resonance peak is removed for stiffness coefficients 600, 800, 1000, 1200 and 1400 N/m, we have implemented virtual damping coefficients of 100, 117, 131, 145 and 157 Ns/m respectively, according to (10) using $m = 5$ kg and $b = 10$ Ns/m. Fig. 13 shows the theoretical frequency responses of constrained dynamics (9).

Fig. 14 shows the force that the user exerts and the displacement in that vertical direction using $K = 1000$ N/m and $B = 131$ Ns/m. Now, the behavior associated to the resonance peak (zone II in Fig. 10) does not exist.

Fig. 15 shows the experimental frequency response of the five experiments. It corroborates that the resonance peaks do not exist when introducing the critical damping for the system. As a consequence, it can be concluded that by choosing the value of the virtual damping a more realistic constrained behavior can be achieved, i.e. independent of the frequency. The user does not feel that he/she is interacting with

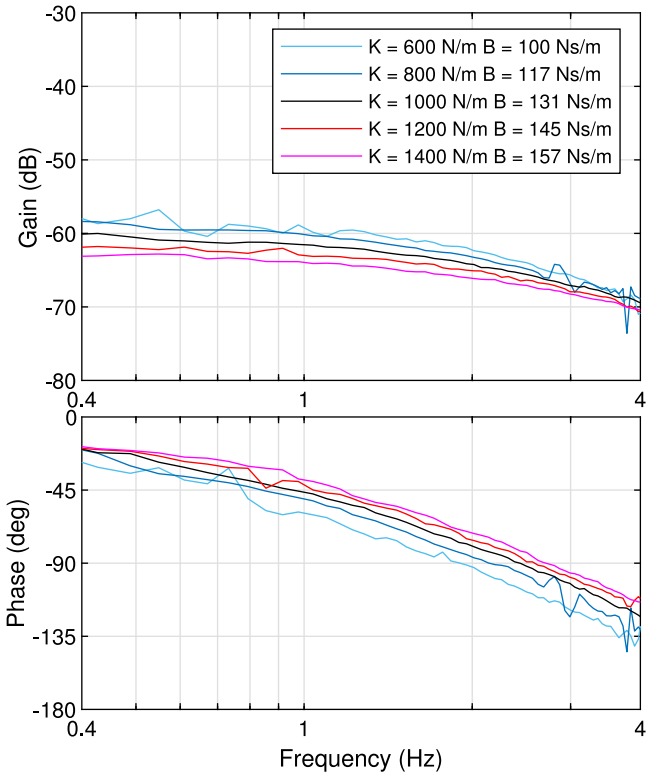

Fig. 15. Experimental frequency response of the system with viscoelastic impedances.

an underdamped second-order system with relatively small apparent inertia.

5. Discussion

When designing a haptic device, two opposing objectives are pursued: complete transparency in free motion (ideally zero impedance) and fully constrained motion in virtual contact (ideally infinite impedance). In the first case, a very small apparent inertia (very low m) is usually sought, and in the second case, a very high virtual stiffness K is usually implemented. However, it has been shown experimentally that having a relatively low inertia in free motion affects the constrained motion because a significant resonance peak will arise. An effective method to correct this undesired effect is to add along with the stiffness K a virtual damping B, which obviously depends on the effective inertia m achieved in the free motion.

It is important to note that, unlike in other works [16–18], we propose adding virtual damping not to guarantee the stability of the virtual contact, but to make the constrained motion more realistic, namely, eliminating the resonance peak.

As for the apparent inertia of the Franka robot, around 5 kg, we have called it relatively small. However, it should be compared with that of other haptic devices. Table 3 presents the apparent inertia of several impedance-type haptic devices. Although there is no obvious relationship between inertia and operational workspace, these characteristics are somehow interconnected. For a rigid link series mechanism to have a large working space, the dimensions of the links must also be considerable. This results in an increase of the moving mass and, consequently, a higher inertia perceived by the user.

If the Franka Emika robot were a reversible mechanism, its apparent inertia would be relatively large, in accordance with its workspace. Since the Franka robot is, in fact, irreversible and its internal controllers are what make it reversible, its apparent inertia should be compared with that achieved by admittance-type haptic devices. For example, the HapticMaster can render different virtual inertias, but not below 2 kg (probably with negligible damping) [21]. The Franka robot's internal controller, which makes it simply reversible, does not achieve comparable transparency. Therefore, we recommend developing a specific admittance control that not only makes the apparent inertia lower but also makes it isotropic.

Table 3
Physical inertia of several haptic devices.

Device	Inertia	Workspace (mm)
PHANToM 1.0 [15]	72 g	160 W × 120 H × 70 D
Omega [15]	220 g	160 ⌀ × 120 L
Delta [15]	250 g	360 ⌀ × 300 L
Mirage F3D-35	300 g	400 W × 300 H × 200 D
Virtuose 6D	1 kg	450 W × 450 H × 450 D
HomeRehab [19]	1.35 kg	800 W × 400 H × 400 D
Excalibur [20]	3.9 kg	300 W × 200 H × 300 D
LHIfAM [16]	5.4 kg	1500 W × 978 H × 385 D

6. Conclusion and future work

The study of the mechanical behavior of the Franka Emika robot was conducted, with emphasis on those parameters that characterize its performance as a haptic device. Experiments were carried out to estimate the dynamic behavior of the device in two scenarios: free motion and high impedance constrained motion.

The apparent inertia in free movement has a high value in comparison with other haptic devices and it is highly anisotropic. As a future work, it is proposed to develop an admittance controller, in order to solve the anisotropy and to reduce the apparent inertia to a moderate value around 2 kg. As for the behavior in constrained motion, a good performance was achieved, without the undesired resonance effect.

CRediT authorship contribution statement

Wilson Brian: Writing – original draft, Software, Investigation, Formal analysis, Conceptualization. **Sebastián Gutiérrez:** Writing – review & editing, Writing – original draft, Investigation, Formal analysis, Conceptualization. **Jorge Juan Gil:** Writing – review & editing, Writing – original draft, Visualization, Validation, Supervision, Investigation, Formal analysis, Conceptualization.

Declaration of competing interest

The authors declare that they have no known competing financial interests or personal relationships that could have appeared to influence the work reported in this paper.

Acknowledgments

The authors would like to thank Marcus Gulinao, from Linköping University, for his contribution in developing the handle for the Franka Emika robot. This design facilitated the execution of experimental trials, thereby improving the evaluation of the robot's performance.

Data availability

Data will be made available on request.

References

[1] Jiang W, jin Zheng J, jun Zhou H, kai Zhang B. A new constraint-based virtual environment for haptic assembly training. Adv Eng Softw 2016;98:58–68. http://dx.doi.org/10.1016/j.advengsoft.2016.03.004.

[2] Lee J, Choi S. Effects of haptic guidance and disturbance on motor learning: Potential advantage of haptic disturbance. In: 2010 IEEE haptics symposium. 2010, p. 335–42. http://dx.doi.org/10.1109/HAPTIC.2010.5444635.

[3] Sveistrup H. Motor rehabilitation using virtual reality. J NeuroEng Rehabil 2004;1. http://dx.doi.org/10.1186/1743-0003-1-10, paper no. 10.

[4] Hirche S, Buss M. Human-oriented control for haptic teleoperation. Proc IEEE 2012;100(3):623–47. http://dx.doi.org/10.1109/JPROC.2011.2175150.

[5] Patel RV, Atashzar SF, Tavakoli M. Haptic feedback and force-based teleoperation in surgical robotics. Proc IEEE 2022;110(7):1012–27. http://dx.doi.org/10.1109/JPROC.2022.3180052.

[6] Wang Y-H, Liu G-Y, Huang G, Wang Y. Variable admittance force feedback device and its human-robot interaction stability. Robot Comput-Integr Manuf 2023;82:102537. http://dx.doi.org/10.1016/j.rcim.2023.102537.

[7] Lawrence DA, Pao LY, Salada MA, Dougherty AM. Quantitative experimental analysis of transparency and stability in haptic interfaces. In: 1996 ASME international mechanical engineering congress and exposition, vol. 58. 1996, p. 441–9.

[8] Colgate J, Brown J. Factors affecting the Z-width of a haptic display. In: Proceedings of the 1994 IEEE international conference on robotics and automation. 1994, p. 3205–10 vol.4. http://dx.doi.org/10.1109/ROBOT.1994.351077.

[9] Knopp S, Lorenz M, Pelliccia L, Klimant P. Using industrial robots as haptic devices for VR-training. In: 2018 IEEE conference on virtual reality and 3D user interfaces. 2018, p. 607–8. http://dx.doi.org/10.1109/VR.2018.8446614.

[10] Franka Robotics GmbH. Product manual franka emika robot. 2021, URL https://franka.de/documents. [Accessed: 7 May 2024].

[11] Franka Robotics GmbH. Robot and interface specifications. 2023, URL https://frankaemika.github.io/docs/control_parameters.html. [Accessed: 7 May 2024].

[12] Canadian Centre for Occupational Health and Safety. Tool Design. 2024, https://www.ccohs.ca/oshanswers/ergonomics/handtools/tooldesign.html. [Accessed: 15 May 2024].

[13] Culinao M, Gutiérrez S, Gil JJ, Brian W. Handle for franka emika robot. 2024, http://dx.doi.org/10.17632/smxyw6psbr.1, Mendeley Data, V1.

[14] Petrea RAB, Bertoni M, Oboe R. On the interaction force sensing accuracy of franka emika panda robot. In: IECON 2021 – 47th annual conference of the IEEE industrial electronics society. 2021, http://dx.doi.org/10.1109/IECON48115.2021.9589424.

[15] Diolaiti N, Niemeyer G, Barbagli F, Salisbury JK. Stability of haptic rendering: Discretization, quantization, time-delay and Coulomb effects. IEEE Trans Robot 2006;22(2):256–68. http://dx.doi.org/10.1109/TRO.2005.862487.

[16] Gil JJ, Sánchez E, Hulin T, Preusche C, Hirzinger G. Stability boundary for haptic rendering: Influence of damping and delay. J Comput Inf Sci Eng 2009;9(1):011005. http://dx.doi.org/10.1115/1.3074283.

[17] Hulin T, Preusche C, Hirzinger G. Stability boundary for haptic rendering: Influence of physical damping. In: 2006 IEEE/RSJ international conference on intelligent robots and systems. Beijing, China; 2006, p. 1570–5. http://dx.doi.org/10.1109/IROS.2008.4650697.

[18] Mashayekhi A, Behbahani S, Ficuciello F, Siciliano B. Analytical stability criterion in haptic rendering: The role of damping. IEEE/ASME Trans Mechatronics 2018;23(2):596–603. http://dx.doi.org/10.1109/TMECH.2018.2797688.

[19] Gil JJ, Ugartemendia A, Díaz I. Rendering virtual inertia in haptic interfaces: Analysis and limitations. In: 2022 IEEE international conference on robotics and automation. Philadelphia, Pensilvania, USA; 2022, p. 8876–81. http://dx.doi.org/10.1109/ICRA46639.2022.9812207.

[20] Adams RJ, Hannaford B. Control law design for haptic interfaces to virtual reality. IEEE Trans Control Syst Technol 2002;10(1):3–13. http://dx.doi.org/10.1109/87.974333.

[21] van der Linde R, Lammertse P. HapticMaster - A generic force controlled robot for human interaction. Ind Robot Int J 2003;30(6):515–24. http://dx.doi.org/10.1108/01439910310506783.

Wilson Brian received his B.Eng. degree in Industrial Engineering from the University of Montevideo, Montevideo, Uruguay, in 2022. He is currently a Ph.D. student at Tecnun, University of Navarra, researching the use of haptic devices for industrial applications.

Sebastián Gutiérrez received his Ph.D. in Automation and Industrial Electronics Engineering from the University of Navarra, San Sebastián, Spain, in 2012, and his M.Sc. from Panamericana University, Aguascalientes, Mexico, in 2007. He is currently an Associate Professor at the University of Navarra. His research interests include robotics, mechatronic systems, wireless sensor networks, solar energy and the Internet of Things.

Jorge Juan Gil received his M.S. and Ph.D. degrees in Mechanical Engineering from the University of Navarra, Spain, in 1997 and 2003, respectively. From 2012 until 2016, he led the Experimental Dynamics and Design Unit of the Applied Mechanics Department of Ceit. Currently, he is Deputy Director of Students and professor of Control Engineering at Tecnun, University of Navarra. His main research interest is robot control and haptic interfaces. In particular, he has experience in developing algorithms for haptic rendering, analyzing the factors affecting the stability of the haptic interaction, and characterizing physical parameters of robot joints.